In vivo mechanical response of thigh soft tissues under compression: a two-layer model allows an improved representation of the local tissue kinematics

Alexandre Segain, Giuseppe Sciumè, Helene Pillet, Pierre-Yves Rohan

In vivo mechanical response of thigh soft tissues under compression: A two-layer model allows an improved representation of the local tissue kinematics

Alexandre Segain [a,*], Giuseppe Sciume [b], Hélène Pillet [a], Pierre-Yves Rohan [a]

[a] *Arts et Métiers Institute of Technology, Université Sorbonne Paris Nord, IBHGC - Institut de Biomécanique Humaine Georges Charpak, HESAM Université, F-75013, Paris, France*
[b] *Arts et Metiers Institute of Technology, Univ. of Bordeaux, CNRS, Bordeaux INP, INRAE, I2M Bordeaux, Av d'Aquitaine, 33607, Pessac, France*

A R T I C L E I N F O

Keywords:
Mechanical characterisation *in vivo*
Pressure ulcer prevention
Ultrasound/Echography

A B S T R A C T

Biomechanical parameters have the potential to be used as physical markers for prevention and diagnosis. Finite Element Analysis (FEA) is a widely used tool to evaluate these parameters *in vivo*. However, the development of clinically relevant FEA requires personalisation of the geometry, boundary conditions, and constitutive parameters. This contribution focuses on the characterisation of mechanical properties *in vivo* which remains a significant challenge for the community. The aim of this retrospective study is to evaluate the sensitivity of the computed elastic parameters (shear modulus of fat and muscle tissues) derived by inverse analysis as a function of the geometrical modelling assumption (homogenised monolayer vs bilayer) and the formulation of the cost function. The methodology presented here proposes to extract the experimental force-displacement response for each tissue layer (muscle and fat) and construct the associated Finite Element Model for each volunteer, based on data previously collected in our group (N = 7 volunteers) as reported in (Fougeron et al., 2020). The sensitivity analysis indicates that the choice of the cost function has minimal impact on the topology of the response surface in the parametric space. Each surface displays a valley of parameters that minimises the cost function. The constitutive properties of the thigh (reported as median ± interquartile range) were determined to be ($\mu = 198 \pm 322\ Pa, \alpha = 37$) for the monolayer and ($\mu_{muscle} = 1675 \pm 1127\ Pa, \alpha_{muscle} = 22 \pm 14, \mu_{fat} = 537 \pm 1131\ Pa, \alpha_{fat} = 32 \pm 7$) for the bilayer. A comparison of the homogenised monolayer and bilayer models showed that adding a layer reduces the error on the local force displacement curves, increasing the accuracy of the local kinematics of soft tissues during indentation. This allows for an increased understanding of load transmission in soft tissue. The comparison of the two models in terms of strains indicates that the modelling choice significantly influences the localization of maximal compressive strains. These results support the idea that the biomechanical community should conduct further work to develop reliable methodologies for estimating *in vivo* strain in soft tissue.

1. Introduction

In various daily life situations (such as lying down, sitting in a wheelchair, wearing a prosthesis or wearing a facemask), soft tissues are compressed against bony prominences. This prolonged compression may result in significant soft tissue injuries, such as deep tissue injuries. These injuries may have a severe impact on patients' quality of life, causing pain, prolonged hospital stays, and difficulty lying on the affected skin. They can also result in a substantial financial burden (Demarré et al., 2015).

Experimental research on tissue biomechanics, carried out on animal models, has demonstrated a correlation between internal tissue strain and tissue damage (Ceelen et al., 2008). However, the direct measurement of biomechanical parameters such as stress and strain is not possible in a non-invasive manner. Therefore, in order to use biomechanical parameters as physical markers for prevention and diagnosis, it is necessary to estimate these quantities from accessible data.

Finite Element Analysis (FEA) has been widely used to evaluate these parameters *in vivo*. For running clinically relevant FEA, personalisation of the geometry, boundary conditions and constitutive parameters is necessary. However, the *in vivo* characterisation of the mechanical properties is rarely conducted and remains a major challenge for the

* Corresponding author.
E-mail address: alexandre.segain@ensam.eu (A. Segain).

biomechanical community. Results of a sensitivity analysis carried out in (Luboz et al., 2014a) showed that Von Mises strains of buttock tissues under compression ranges from 1.5% to 54.8% for muscle tissue and from 22.8% to 92.7% for adipose tissue with the change in equivalent Young's Modulus from 40 kPa to 160 kPa and from 5 kPa to 40 kPa respectively.

Numerous methodologies have been proposed in the literature to investigate the mechanical response of muscle and fat tissues under different external mechanical loading conditions both *in vivo* and *ex vivo*. *Ex vivo* analysis, in particular, has yielded significant insights through traditional mechanical characterization techniques such as uniaxial and biaxial tensile tests (Gras et al., 2012; Sommer et al., 2013), pure shear (Morrow et al., 2010), plain strain compression (Böl et al., 2012; Calvo-Gallego et al., 2020), bulge tests (Diab et al., 2020) and indentation tests (Haddad et al., 2020; Kim and Srinivasan, 2005). However, the *in vivo* condition differ from the *ex vivo* experiments carried out, where individual components such as fat, muscle and bone are isolated. Considering the substantial intra-individual differences *in vivo* and also between *in vivo* and *ex vivo* conditions, this question is not trivial. It follows that several attempts have been proposed to non-invasively identify mechanical properties of soft tissues *in vivo* (Fougeron et al., 2020; Luboz et al., 2014; Mak et al., 1994; Tran et al., 2007). Aspiration-based set-ups have received a lot of attention for the characterisation of the quasi-static mechanical response of the superficial soft tissues *in vivo* (Barbarino et al., 2011; Hendriks et al., 2003; Luboz et al., 2014b). However, they are limited by construction to the first layers of tissue. On the other hand, indentation-based methods have been proposed to evaluate the non-linear stiffness of deep tissues (Affagard et al., 2015; Avril et al., 2010; Isogai et al., 2022).

Indentation-based methods (Fougeron et al., 2020; Makhsous et al., 2008) generally assume an equivalent single layer tissue. However, several *in vivo* experiments observed significant differences in the mechanical behaviour of fat and muscle tissues during compression (Al-Dirini et al., 2016; Call et al., 2017; Doridam et al., 2018; Hatt et al., 2023; Isogai et al., 2022; Sonenblum et al., 2015). Hence it is not pertinent to model soft tissue as a single homogeneous layer, this strong assumption may largely contribute to errors in the estimated behaviour. Only few studies investigated the characterisation of each tissue in a separated manner (Affagard et al., 2015; Avril et al., 2010; Silber and Then, 2013; Then et al., 2012). All these studies rely on an indentation testing using imaging modalities, most frequently Magnetic Resonance Imaging (MRI) or UltraSound Imaging (USI), combined with an inverse method, typically Finite Element Updating, and are thus based on an optimisation procedure. As emphasised in a recent article by (Oddes and Solav, 2023), the importance of verifying and quantifying the uniqueness of the solution for a given cost function was highlighted. This point is never discussed in most of articles using an optimisation procedure.

The aim of this study is to evaluate the sensitivity of the material parameters of fat and muscle estimated by inverse analysis with respect to the geometrical modelling assumption (homogenised monolayer vs bilayer) and the formulation of the cost function. The hypothesis of this work is that a bilayer model allows a better representation of the force/displacement relationship of the soft tissue submitted to indentation at the global (whole tissue) and local (each tissue separately) scale. To test the reliability of this hypothesis, we will build upon the *in vivo* force-displacement data previously collected in our group in (Fougeron et al., 2020).

2. Materials and methods

The proposed methodology is briefly outlined here. A brief description of the experimental material previously collected in our group in (Fougeron et al., 2020) is first given in section 2.1. Section 2.2.1. outlines the methodology employed to extract the experimental force-displacement response for each tissue layer (muscle and fat). The construction and post-processing procedure of both the reference homogenised monolayer FE model and bi-layer model are presented in sections 2.2.2. and 2.2.3. respectively. To avoid the problem of local minima that could lead to a misidentification of the material parameter these models are used in sections 2.2.4 and 2.2.5. respectively to explore the parametric space of the constitutive parameters. To quantify the agreement between the experimental and numerical values, several cost functions are introduced in section 2.2.6.

2.1. Materials (initial dataset collected in a previous work)

For the sake of clarity, the description of the participants and description of the data collection (Fougeron et al., 2020) is briefly recalled hereunder in sections 2.1.1 and 2.1.2. respectively. For a detailed explanation, the reader is invited to read the original article.

2.1.1. Participants

The acquisition protocol received the approval by the local ethics committee (Comitée de-Protection des Personnes CPP NX06036). Seven healthy volunteers participated in the experiments. The subjects were aged between 23 and 41 years old and had body mass indices comprised between 21.4 and 24.3 kg/m^2. Their data are summarized in Table 1. The original research of (Fougeron et al., 2020) explored two muscle configurations: contracted and relaxed and the data were acquired by two different operators. For this study, only the measurements collected by the first operator in the relaxed configuration were analysed.

2.1.2. Data collection

The participants were instructed to lie on a bed with their leg muscles in a relaxed state. The mid-thigh was compressed on its anterior and lateral section (See Fig. 1 for a scheme of the anatomical location) until an observable stiffening of the tissue was detected, which corresponded to a load between 30 N and 80 N. A linear ultrasound probe of 8 MHz central frequency (SuperLinearTM SL 15-4, Aixplorer; SuperSonic Imagine, Aix-en-Provence, France) was used for the examination. The probe was connected to a 200 N force sensor (3134—Micro-Load Cell (0–20 kg)—CZL635, GoTronic, Paris, France) and to an amplifier (Sparkfun, SEN-13879, SparkFun Electronics, Niwot, Colorado). An Arduino card (Arduino, UNO REV 2 V4.0) was used to gather data. Short ultrasound clips were recorded using the echograph system (Aixplorer, SuperSonic Imagine, France), during the acquisitions. The ultrasound settings were adjusted for each subject to clearly distinguish the femur on the ultrasound clips. During each acquisition, the operator performed at least 10 cycles of loading and unloading of the tissue at a self-selected loading speed.

2.2. Methods

2.2.1. Extraction of the experimental force/displacement curves

The procedure for the extraction of the global force/displacement curve (i.e. assuming a single layer of tissue) is fully described in (Fougeron et al., 2020). First, the displacement of the skin with respect to the bone surface were assessed from the ultrasound images. Briefly, an operator defined a rectangular region of interest containing the bone contour by manually selecting two points (rectangle a in Fig. 2 A). Then

Table 1
Anthropometric measurement of the subjects.

Subject	BMI (kg/m^2)	Mean initial thickness (mm)	Soft tissue ratio (adipose thickness/muscle thickness)
1	21.4	52.0	0.36
2	21.8	40.6	0.23
3	21.8	49.9	0.27
4	21.7	49.4	0.15
5	22.3	46.1	0.15
6	23.8	43.5	0.13
7	24.3	50.8	0.34

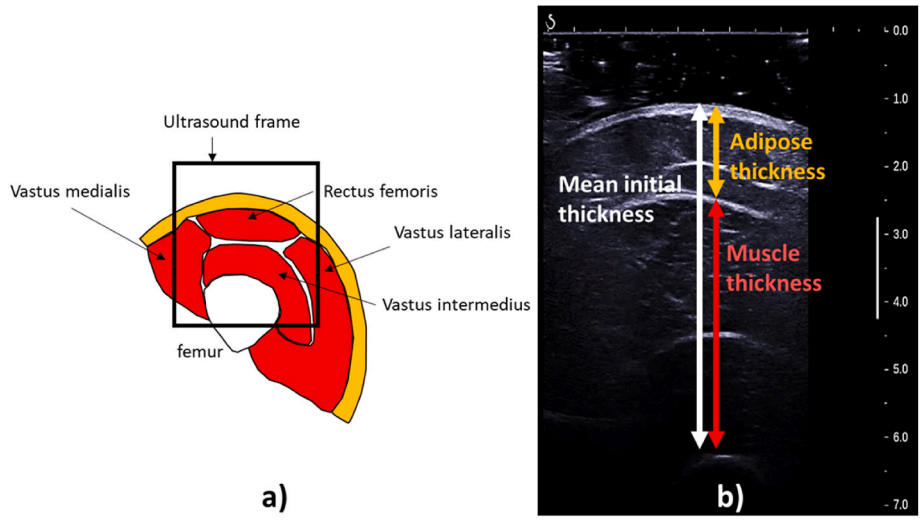

Fig. 1. a) anatomical scheme of the anterior thigh. b) Ultrasound image taken in the undeformed configuration. A thick layer of gel allows us to guarantee that the tissue is not compressed during the acquisition. The different layers' thicknesses are measured on this image.

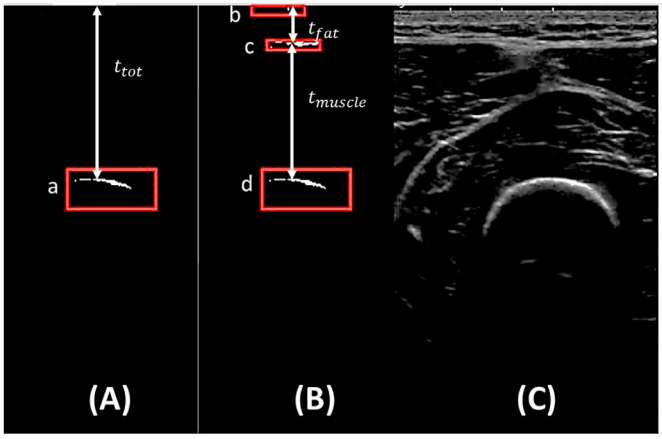

Fig. 2. *(A) example of the tracked interface in the research from* (Fougeron et al., 2020) *a: Tracked bone contour. (B) example of the tracked interfaces in this research b/Skin, c/muscle/adipose tissue interface d/femur. (C), associated B-mode ultrasound image.*

the ultrasound images from the ultrasound frames were converted into black and white using a threshold. The vertical displacement of the bone was estimated by tracking the position of the highest point on each black and white frame. Force and displacement signals were then paired using peak detection to construct the force/displacement curves.

In this contribution, the methodology was extended to simultaneously track the bone contour, the muscle/fat interface and the skin contour, enabling the acquisition of the adipose tissue and muscle tissue thicknesses respectively in each frame (Fig. 2 B). The peaks of the global displacement signal were used to pair force and local thickness signals which resulted in force/displacement curves for the whole tissue and for the muscle and adipose tissue, corresponding to the global and the local response of the tissue. From the curves of each cycle, the mean curve of each acquisition was computed.

2.2.2. Construction of the monolayer and bilayer finite element models

For the monolayer model, soft tissue was considered as a cylinder with dimensions that were adjusted based on the total thickness measured on the ultrasound images in the undeformed configuration for each participant. For the bilayer model, soft tissue was modelled as two concentric cylinders. The dimensions were adjusted based on the thickness of each tissue. For both models, the femur was not included in the simulation and was represented as a hole in the muscle cylinder with fixed boundary conditions on the inner nodes of the hollow cylinder. To reduce the computational cost, only a quarter of the cylinder was considered, and symmetric boundary conditions were assigned to the surface of symmetry. The geometry of the model can be seen on Fig. 3. It was meshed using linear hexahedral elements with hybrid formulation (C3D8H) with an edge size of maximum 4 mm and at least 4 elements in the depth of the adipose tissue. Convergence analysis showed that refining the mesh did not change the force displacement response (less than 5%). The meshing tools available in ABAQUS® were used to generate the computational mesh of the reconstructed geometry. The soft tissue computational domain was divided into two subdomains corresponding to muscle and adipose tissue respectively, which ABAQUS/CAE could mesh using quadrilateral elements with the structured meshing techniques. This strategy ensured that the muscle and fat tissues shared the same nodes at the interface. Consequently, no mesh constraint or interaction properties were defined at the interface.

The tissues mechanical response was modelled as a first order hyperelastic model (Ogden, 1973) using the following strain energy density.

$$\Psi = \frac{2\mu}{\alpha^2}\left(\overline{\lambda_1}^{\alpha} + \overline{\lambda_2}^{\alpha} + \overline{\lambda_3}^{\alpha} - 3\right) + \frac{1}{D}\left(J^{el} - 1\right) \quad (1)$$

Where Ψ is the strain energy density, μ the initial shear modulus, α the exponent, $\overline{\lambda}_i$ the deviatoric principal stretch, D the incompressibility parameter and J^{el} the elastic volume ratio. The value of the incompressibility parameter D was defined using the relation of (Mott et al., 2008)(Equation (2)).

$$D = \frac{2}{\kappa} \approx \frac{3(1-2\nu)}{\mu(1+\nu)} \quad (2)$$

The tissue was assumed to be quasi-incompressible, and a Poisson's ratio of $\nu = 0.49$ was used.

The nodes corresponding to the femur were tied. In all the simulations, the indentation of thigh soft tissues was performed by applying a displacement of 25 mm (corresponding to the mean value of the total indentation) to the ultrasound probe. Previous testing showed that this input displacement was sufficient to observe the non-linear rigidification of the simulated force/displacement relationship, whereas imposing a higher displacement to the probe was often detrimental for the convergence of the models with thin tissue layers.

The interaction between the skin and the ultrasound probe was

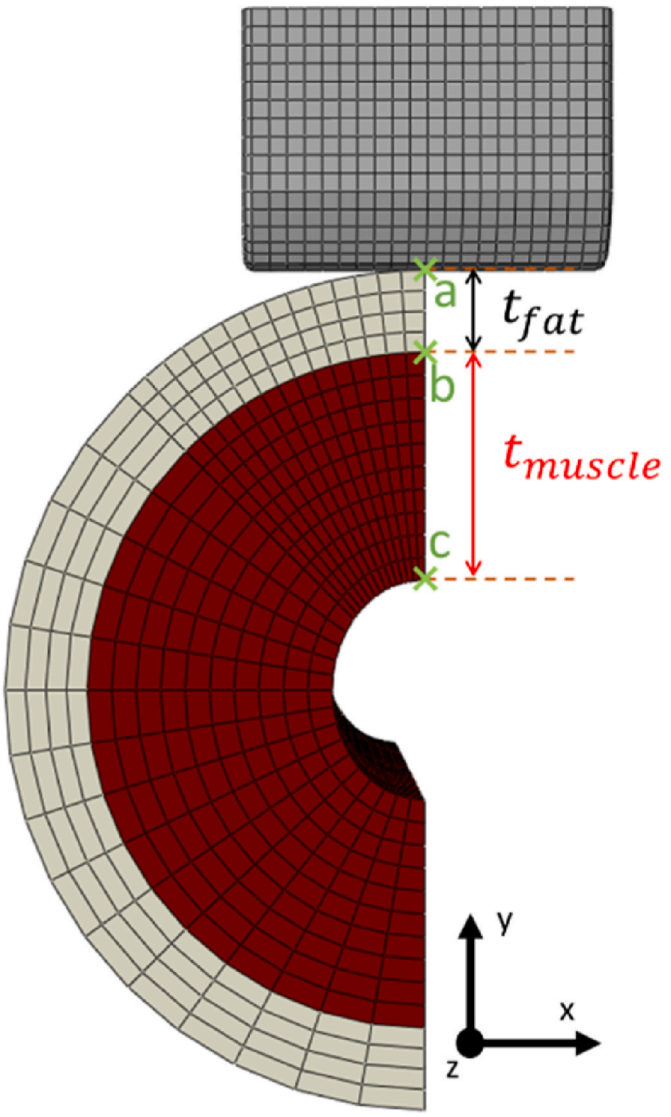

Fig. 3. Localization of the nodal points for the extraction of the displacement a) nodal point on Skin b) nodal point at the muscle/fat Interface c) nodal point on the inner cylinder representing the muscle.

enforced using the default ABAQUS® parameters in the normal direction and using a frictionless contact in the tangential direction. The resolution was performed via an implicit scheme. The default convergence criteria in ABAQUS/Standard were used.

2.2.3. Post processing of the numerical results

The simulations were post processed to extract both the global and local force/displacement curves and the local tissue strain in both the muscle tissue and adipose tissue regions. The variation of thickness of the muscle layer (t_{muscle}) was extracted as the difference of vertical displacement (y direction on Fig. 3) of the points on the outer and inner cylinder representing the muscle tissue (respectively points b and c on Fig. 3). The variation of thickness of the adipose layer (t_{fat}) was extracted as the difference of vertical displacement of the points on the skin and the interface (a and b on Fig. 3). Finally, the global variation of thickness was extracted as the difference of vertical displacement of the points on the skin and the inner radius of the cylinder representing the muscle (points a and c on Fig. 3). Force displacement curve was then obtained by fitting a 5-degree polynomial to the points obtained for the different computation steps.

The principal stretches λ_i $(i = 1,2,3)$ and the principal Green-Lagrange E_i $(i = 1,2,3)$ strains were computed from the ABAQUS Logarithmic strains. The principal shear strains were then computed as:

$$E_{shear} = \frac{1}{2}*\max(|E_1 - E_2|, |E_2 - E_3|, |E_3 - E_1|) \quad (3)$$

The third principal strain component E_3 corresponds to the principal compressive strain. This quantity will be referred to hereafter as E_{comp}.

2.2.4. Exploration of the parametric space (homogenised monolayer)

An analysis of the parametric space (μ,α) was carried out to examine the effect of the constitutive parameters (μ,α) on the local tissue stress/strain response and the global force-displacement response. This methodology has been used to avoid problems of local minima and have an idea of the effect of the material parameters on a representative part of the parametric space. According to the literature, the values of the exponent coefficient α varies from 3 (Omidi et al., 2014)to 35 (Gras et al., 2012). To be consistent with the values used in the article from (Oddes and Solav, 2023), the range of values for the α coefficient has been set to [1,37]. The reported literature values of shear modulus μ vary from 20 Pa (Calvo-Gallego et al., 2020; Vaidya and Wheatley, 2020) to 45 kPa (Gras et al., 2012) However, after first attempts, simulations with high values of shear modulus did not represent correctly the behaviour of the experimental force displacement curve. As a result, the range of variation has then been set to [0.01,25] kPa.

As the literature presents mostly values between 0.01 kPa and 1 kPa (Affagard et al., 2015; Avril et al., 2010; Calvo-Gallego et al., 2020; Hatt et al., 2023; Omidi et al., 2014; Samani et al., 2003; Silber and Then, 2013; Sommer et al., 2013; Tran et al., 2007) on adipose tissue, (Chawla et al., 2009; Hatt et al., 2023; Moerman et al., 2017; Oomens et al., 2013; Then et al., 2012; Vaidya and Wheatley, 2020) on muscle tissue, it seemed relevant to perform a fine exploration of the 0.01–1 kPa interval by using a logarithmic scale to select 52 values of the shear modulus. A total of 2072 simulations were performed for each subject.

2.2.5. Exploration of the parametric space (bilayer)

An identical approach was employed to examine how the constitutive parameters $(\mu_{muscle}, \alpha_{muscle}, \mu_{fat}, \alpha_{fat})$ impacts the global force-displacement response and the local tissue stress/strain response when the muscle and fat tissues are differentiated.

In order to limit the number of simulations and therefore the computation time, the number of values for each parameter was set to 15 for each of the 4 degrees of freedom. In total, the number of simulations for the parametric analysis was $n_{simu} = (15)^4 = 50625$ simulations per subject.

The same variation ranges were used for both tissue layer. The exponential coefficient values were chosen by rounding 15 values that are linearly spaced between 1 and 37. The shear modulus values were selected by taking one point out of four from the values presented in 2.2.4.

2.2.6. Cost functions

Depending on the objective, different metrics can be used to measure the distance between the numerical and experimental curves.

In this paper, seven cost functions (noted J_i $i = [1;7]$) have been defined and are described in equations (4)–(10) to quantify the impact of the constitutive parameters on the global force-displacement response.

The first cost function denoted J_1 corresponds to the Root Mean Square Error between the experimental and numerical force displacement curves, giving an information on the global mismatching.

To ensure that the non-linearity of the experimental force/displacement curve is represented the cost function J_2 was developed to consider only the initial and final slopes of the curves. As it might be important to represent in a correct manner the fully compressed state, cost function J_3 was defined using the value of the force in the initial and fully-deformed configuration.

Finally, the cost function J_4 J_5 J_6 and J_7 were constructed upon the

previous ones to see if the additional information could help for the convergence.

$$J_1 = \frac{1}{mean(\hat{\boldsymbol{f}})} * \sqrt{\frac{1}{n}\sum_{i=1}^{n}(f_i - \hat{f}_i)^2} \tag{4}$$

$$J_2 = \sqrt{\left(\frac{p_{min} - \hat{p}_{min}}{\hat{p}_{min}}\right)^2} + \sqrt{\left(\frac{p_{max} - \hat{p}_{max}}{\hat{p}_{max}}\right)^2} \tag{5}$$

$$J_3 = \sqrt{\left(\frac{f_{min} - \hat{f}_{min}}{\hat{f}_{min}}\right)^2} + \sqrt{\left(\frac{f_{max} - \hat{f}_{max}}{\hat{f}_{max}}\right)^2} \tag{6}$$

$$J_4 = J_1 + J_2 \tag{7}$$

$$J_5 = J_1 + J_3 \tag{8}$$

$$J_6 = J_2 + J_3 \tag{9}$$

$$J_7 = J_1 + J_2 + J_3 \tag{10}$$

Where $\wedge$ denotes an experimental value, and bold characters denotes a vector. f stands for force and p stands for the slope. n is the number of experimental data points.

For the monolayer model, the cost functions were evaluated on the global force/displacement curve. As the local kinematic remains of

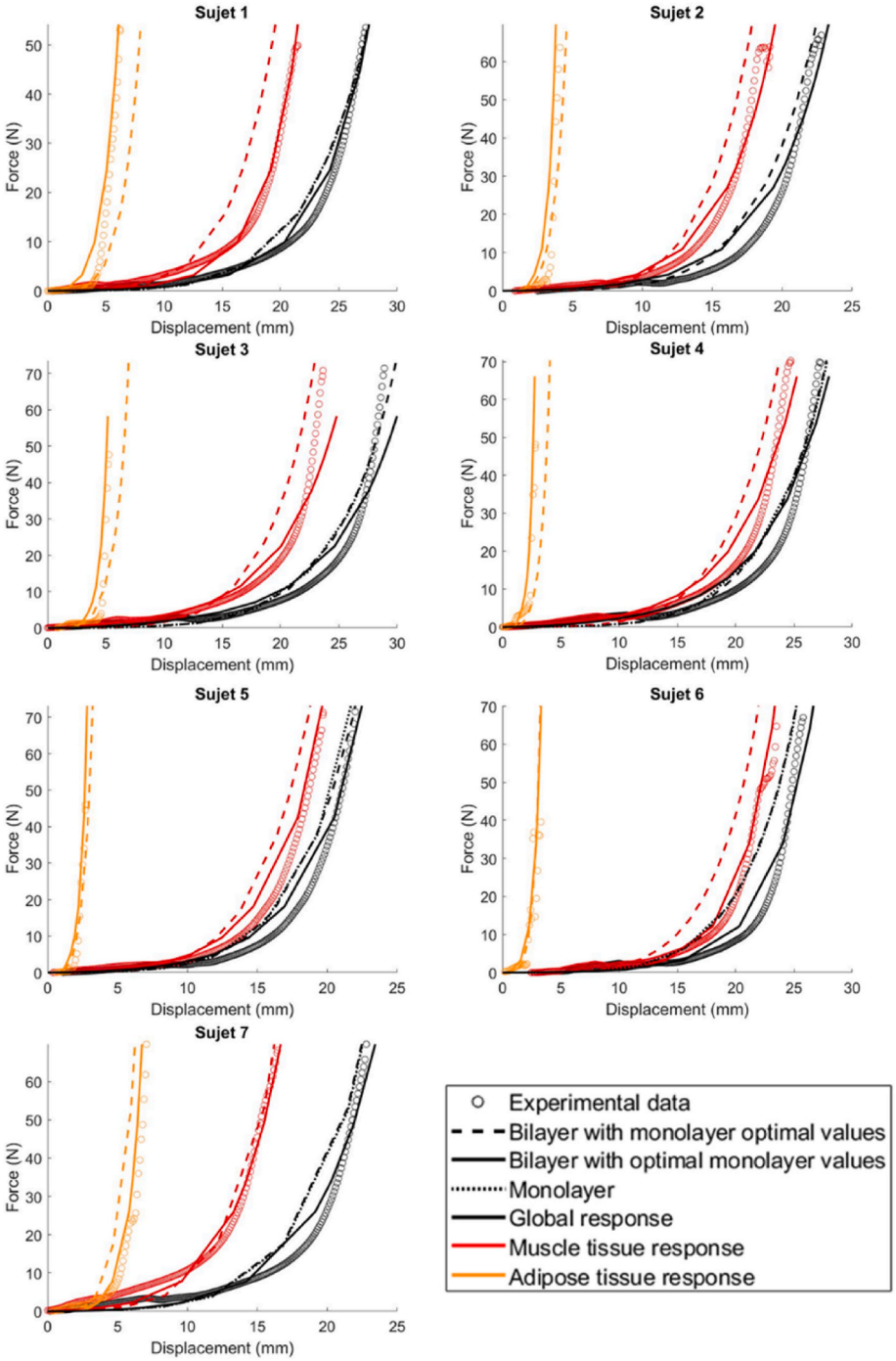

Fig. 4. Experimental and best numerical force-displacement response for the different participants.

major importance for the bilayer model, cost functions were computed on the muscle and fat tissue layer, and the best set of parameters was considered as the one that minimized the sum of the errors on the muscle (called J_{muscle}) and on the adipose tissue (called J_{fat}).

$$J_i^{Bilayer} = J_i^{muscle} + J_i^{fat} \tag{11}$$

In order to compare the results obtained for the mono and bilayer models, simulations were performed using the bilayer model where both layers were assigned the material properties that minimises the cost function on the explored parametric space using the monolayer model. The distance between numerical and experimental force displacement curves was then evaluated for the global, the muscle and the adipose tissue (named J, J_{muscle} and J_{fat} respectively).

Only simulations that achieved 95% of the maximum experimental displacement were post-processed. For the simulations that did not converge, only few data points were existing on the force displacement curve, all located in the part of the curve that corresponds to low displacement. Thus, the rest of the force displacement curve corresponding to high displacement values was extrapolated instead of interpolated. This extrapolation made the accuracy of the cost function questionable for simulations that did not converge, and they were thus not considered.

2.2.7. Statistical analysis

Because of the low sample size, the normality of the distributions were not tested. Data were reported per parameter and per group as median ± interquartile range.

3. Results

3.1. Experimental and numerical force displacement curves

The experimental and numerical force-displacement responses obtained for the mono and bilayer models for the different participants are reported in Fig. 4. The global tissue (skin to bone), muscle tissue layer, and adipose tissue layer responses are represented by the black, red, and yellow lines respectively. The median maximal values of the change of thickness of the different layers are 25.9 ± 4.5 mm, 21.5± 4.3 mm and 4.2 ± 3.1 mm for the global response, muscle layer and fat layer respectively.

3.2. Monolayer model: impact of the choice of the cost function on the best set of parameters

The evolution of the response surface in the parametric space (μ, α) is given in Fig. 5 for subject 1. Similar trends can be observed for the other subjects and are provided in supplementary material for the reader. Cold colours correspond to low values of the cost function (the numerical and experimental force/displacement curves are similar) whereas hot colours correspond to set of parameters for which the distance between the numerical and experimental force displacement curve is high. All response surfaces exhibit a valley, indicating absence of multiple local minima within the explored space of the cost function.

The best force-displacement curves obtained using each of the seven cost functions considered are given in Fig. 6 for subject 1. Similar trends can be observed for the other subjects and are provided in supplementary material for the reader.

Fig. 7 details the response surface for the seven participants based on the J1 cost function (RMSE between the experimental and the simulated force/displacement curves). It can be observed that a similar behaviour is obtained for all the subjects, with a valley of sets of parameters corresponding to low values of the cost function. For 5 subjects out of 7, the value of the α parameter corresponding to the minimal error is 37.

A comparison of the results obtained for three sets of parameters in the valley for the subject 1 displayed as white circles on Fig. 7 can be seen on Fig. 8. The force-displacement curves expose a similar behaviour. The curves obtained for the following sets of parameters ($\mu = 229\ Pa, \alpha = 37$) and ($\mu = 404\ Pa, \alpha = 29$) are even superimposed. The curve obtained with the set of parameters ($\mu = 948\ Pa, \alpha = 20$), is superimposed with the two others for low values of displacement but a gap appears when the displacement becomes taller than 22 mm.

The location of the maximal compressive and shear strain is the same for all set of parameters. However, it can be noticed that the higher the value of the exponential coefficient, the higher the maximal compressive strain is. The maximal compressive strain E_{comp} increases from −0.40 to − 0.43, contrarily to the maximal value of the shear strain that de-

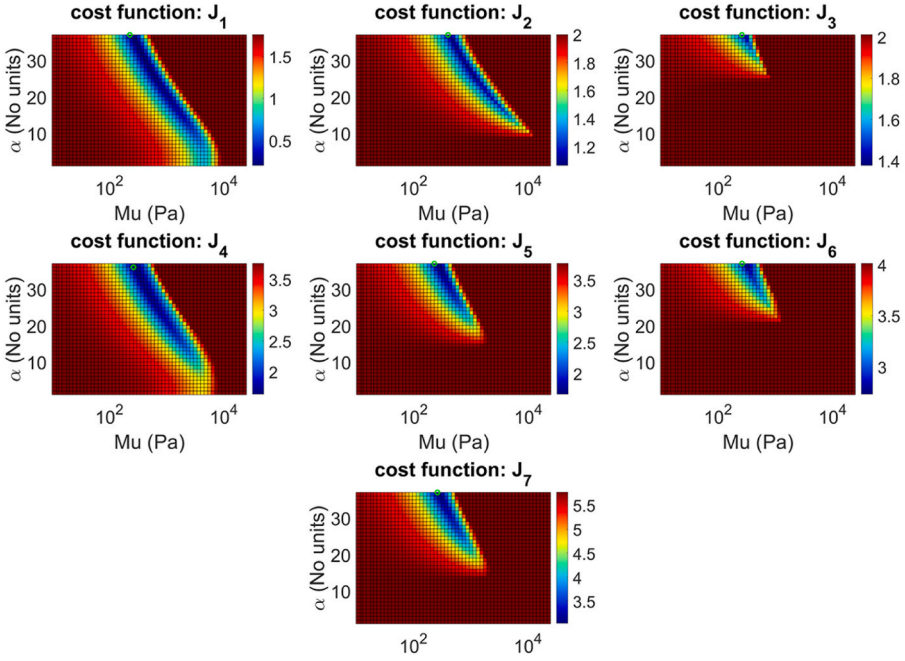

Fig. 5. Evolution of the different cost functions in the parametric space for the subject n°1. The green circle corresponds to the minimal value of the cost function throughout the response surface.

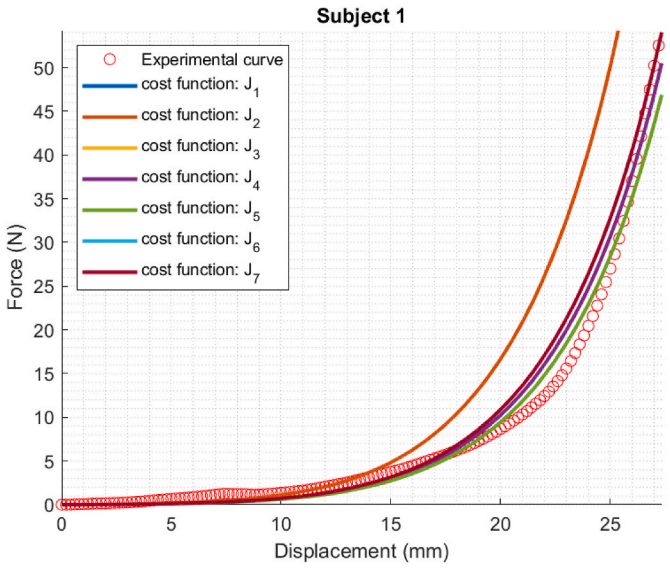

Fig. 6. Comparison of the different force displacement curves obtained using the best set of parameters of the different cost functions.

creases from 0.32 to 0.16, when the exponential coefficient α raises from 20 to 37.

3.3. Bilayer model: exploration of the 4-dimensional parametric space

For the bilayer model, the parametric space has 4 dimensions $\left(\mu_{muscle}, \alpha_{muscle}, \mu_{fat}, \alpha_{fat}\right)$ and the response surface is encoded in a 4D hypercube. To provide a visualisation, the evolution of the response surface intersecting planes based on the J1 cost function (RMSE between the experimental and the simulated force/displacement curves) are given in Fig. 9 for subject 1. Valleys are visible in the three dimensions of the cube, demonstrating the absence of multiple minima in these planes.

The set of parameters minimizing the cost function and the associated values of cost function can be found in Table 2. In this table, the two first columns correspond to the subject ID and the model. The four in the middle correspond to the best set of parameters (μ and α) for each tissue layer. Finally, the three last columns correspond to the minimal value of the cost functions J_1 for the global, the muscle and the fat force-displacement curves.

As it can be seen on Table 2, the bilayer model allows to reduce the gap between the simulated and experimental force/displacement curves for the muscle and adipose tissue. Also, the bilayer model allows to reduce for 4 subjects out of 7 the distance between the global force/displacement curves.

It can be noticed that in the case of the bi-layer model, the best value of initial shear modulus of the muscle tissue (μ_{muscle}) is 1.675 kPa for 5 subjects out of 7.

3.4. Impact of the choice of modelling choice (mono- or bilayer) on the internal strain distribution

Fig. 10 presents the distribution of the compressive logarithmic strain predicted by the monolayer FE model (left) and the bilayer FE model (right) for subject 1. The localization of the maximum compressive strain, as predicted by both the monolayer FE model and the bilayer model, was observed in the adipose tissue region immediately below the probe and in the muscle tissue, respectively. This highlights the substantial impact of the modelling assumptions.

The maximal compressive strain E_{comp} in the fat and muscle tissue region is -0.41 ± 0.04 and -0.43 ± 0.02 for the bilayer configuration and -0.44 ± 0.01 and -0.43 ± 0.02 in the monolayer configuration.

Fig. 11 presents the distribution of the shear logarithmic strain in the X–Y plane predicted by the monolayer FE model (left) and the bilayer FE model (right) for subject 1. The localization of the maximum shear strain does not seem to be impacted by the modelling choice; however, it can be noticed that the range of values went from [−0.29,0.54] to [−0.61,0.70].

The maximal shear strain E_{shear} in the fat and muscle tissue region is 0.24 ± 0.03 and 0.32 ± 0.09 for the bilayer configuration and 0.16 ± 0.02 and 0.19 ± 0.001 in the monolayer configuration.

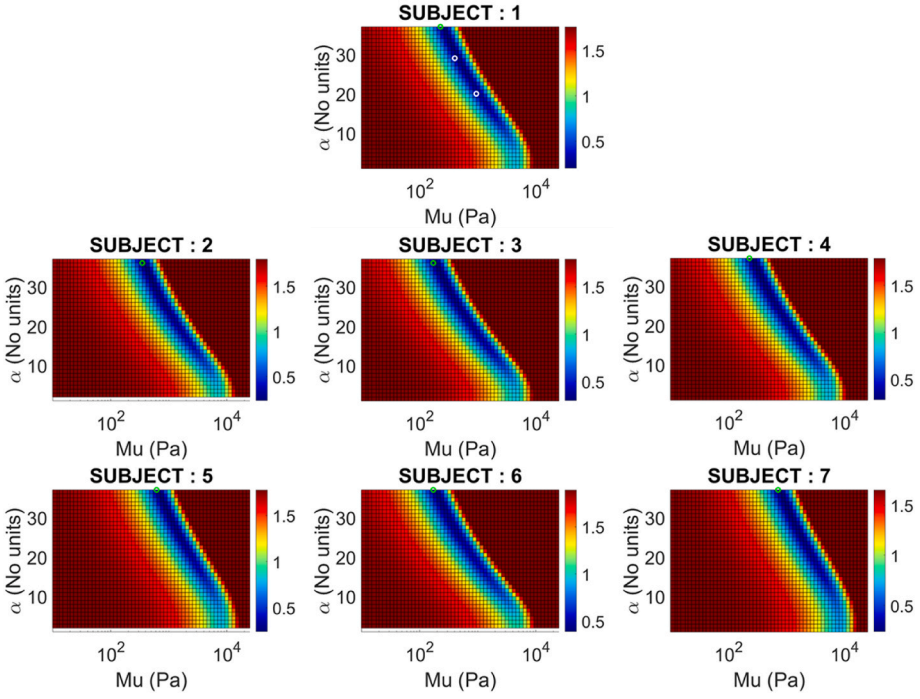

Fig. 7. Evolution of the cost function J1 (corresponding to the root mean square error) in the parametric space for the different subjects. The white circles on subject 1 corresponds to the points used to compare results in the valley.

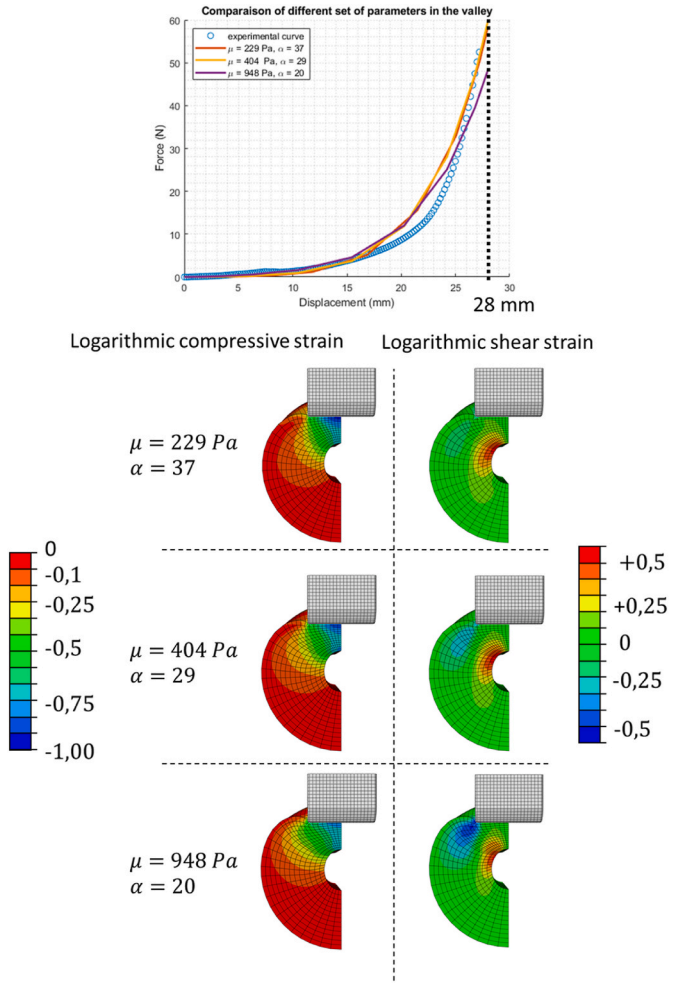

Fig. 8. Comparison of the force displacement curve (top) and strain in the totally deformed configuration (bottom) for the different sets of parameters in the valley.

4. Discussion

The objective of this retrospective study was to assess the sensitivity of the computed elastic parameters, specifically the shear modulus of fat and muscle tissues, derived by inverse analysis as a function of the geometrical modelling assumption (homogenised monolayer vs bilayer) and the formulation of the cost function. The methodology presented relies on the extraction of the experimental force-displacement response for each tissue layer (muscle and fat) and construct the associated Finite Element Model for each volunteer, based on data previously collected in our group (N = 7 volunteers) reported in (Fougeron et al., 2020). The models were then used to explore the parametric space of the constitutive parameters to examine the effect of these parameters on the local tissue stress/strain response and the global force-displacement response and to quantify the agreement between the experimental and numerical values using several cost functions. This methodology is complementary to other existing methodologies to characterize soft tissues mechanical properties such as the use of Kalman filters (Song et al., 2023; Zhu et al., 2021, 2023).

The thigh's constitutive properties (reported as median ± interquartile range) were determined to be ($\mu = 198 \pm 322\ Pa, \alpha = 37$) for the monolayer and ($\mu_{muscle} = 1675 \pm 1127\ Pa, \alpha_{muscle} = 22 \pm 14, \mu_{fat} = 537 \pm 1131\ Pa, \alpha_{fat} = 32 \pm 7$) for the bilayer in 7 subjects. This represents significant progress. Most studies based on optimisation procedures only present results for one subject. (Affagard et al., 2014; Al-Dirini et al., 2016; Avril et al., 2010; Then et al., 2012; Tran et al., 2007). Experimental force/displacement curves show a similar behaviour to that presented in (Hatt et al., 2023; Isogai et al., 2022; Silber and Then, 2013). Muscle tissue deforms less during the first few millimetres of compression and endures more deformation than adipose tissue. This is consistent with the experimental data provided in Appendix A.

As shown in Fig. 5, the choice of the cost function does not appear to affect the topology of the response surface, and none of the cost functions produce multiple minima. However, as demonstrated in Fig. 6 Fig. 6, the choice of cost function can impact the best result that can be obtained, resulting in various force/displacement responses. Therefore, the definition of the cost function should be based on the relevant criteria of interest. The study required a comprehensive model of the thigh soft tissue kinematics. Therefore, the cost function J1, which measures the root-mean-square error (RMSE) between two curves, was used to compare the homogenised monolayer and bilayer models.

For each subject, the cost function J1's response surface displays a

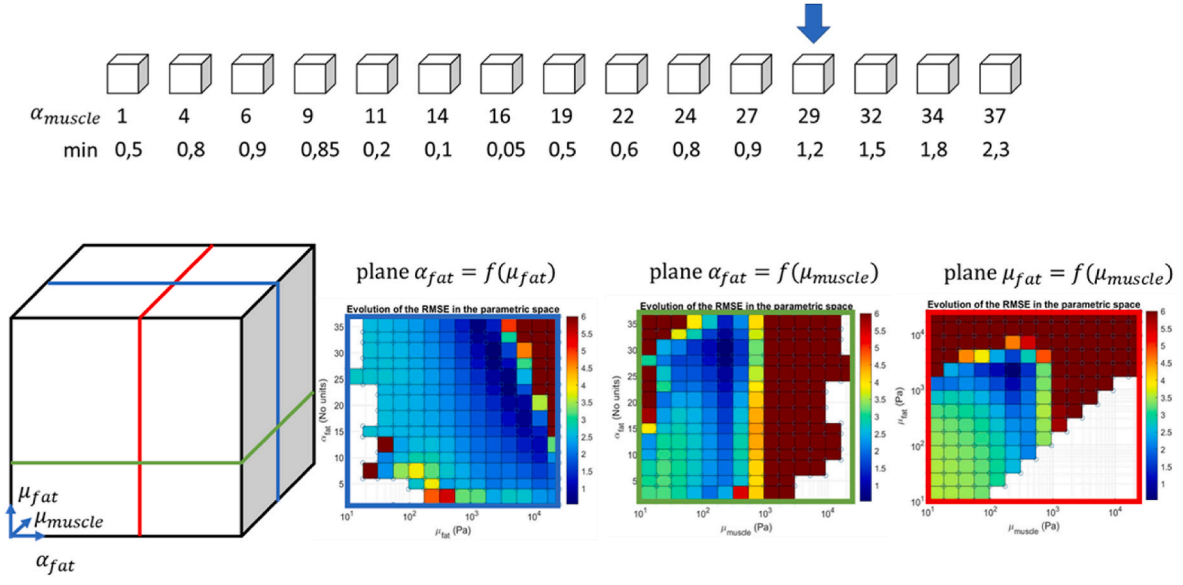

Fig. 9. Evolution of the cost function J1 in the 4D parametric space for the bilayer model of the subject 1.

Table 2
Set of parameters minimizing the cost function and associated values of the cost function.

		μ (Pa)		α		J	J_{muscle}	J_{fat}
		Muscle	Fat	Muscle	Fat			
SUBJECT - 1	Monolayer	198		37		0,251	0,940	1524
	Bilayer	172	1675	29	29	0,191	0,135	0,400
SUBJECT - 2	Monolayer	264		37		0,244	0,429	1174
	Bilayer	1675	537	16	32	0,501	0,236	0,341
SUBJECT - 3	Monolayer	129		37		0,415	0,418	1743
	Bilayer	1675	172	11	37	0,414	0,362	0,810
SUBJECT - 4	Monolayer	198		37		0,322	0,428	1615
	Bilayer	1675	537	14	37	0,390	0,331	0,408
SUBJECT - 5	Monolayer	537		37		0,229	0,388	0,949
	Bilayer	1675	948	22	32	0,292	0,187	0,427
SUBJECT - 6	Monolayer	129		37		0,492	0,167	0,612
	Bilayer	172	1675	29	16	0,452	0,140	0,287
SUBJECT - 7	Monolayer	619		37		0,229	0,263	0,993
	Bilayer	1675	304	27	37	0,105	0,163	0,237

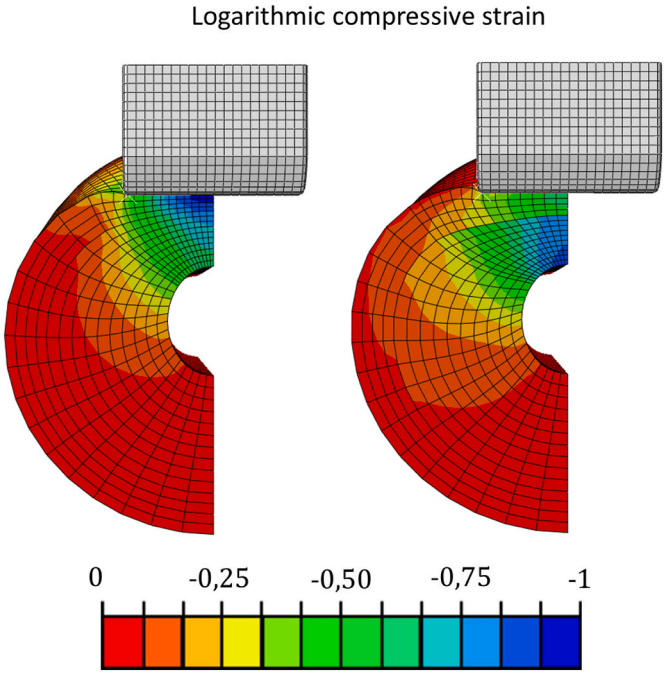

Fig. 10. Repartition of the compressive strain on the models left monolayer model right bilayer model.

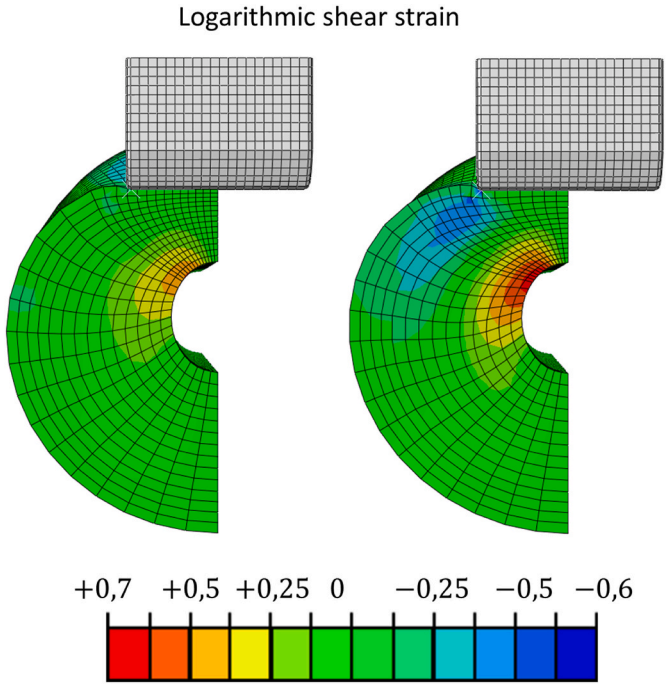

Fig. 11. Repartition of the in-plane shear strain on the models left monolayer right bilayer.

valley where the constitutive parameters correspond to a low error between the numerical and experimental force displacement curve (see Fig. 7). This valley is similar to the one observed in (Oddes and Solav, 2023). In this paper, they explore the parametric space to determine the feasibility of identifying the constitutive parameters of an Ogden law from a force/displacement curve obtained using a reference simulation. Identifying the constitutive parameters of an Ogden law using only the global force displacement response may not be ideal. The authors proposed using additional information about the tissue strain and showed that this reduced the size of the valley. However, obtaining this type of data through experimentation is particularly challenging. Although attempts have been made to deduce the displacement field from ultrasound recordings (Doridam et al., 2018; Vergari et al., 2016), the inadequate quality of ultrasound recordings on the thigh and the potential out-of-plane motion (Mukhina et al., 2022) has resulted in an absence of any reliable technique. Therefore, additional investigations are necessary to estimate the *in vivo* displacement field during indentation.

In this article, the best set of parameters was identified at the limit of the observed range in the literature, indicating that the overall best set of parameters might be out of the explored range. The explored range is based on the values obtained in the literature based on optimisation procedures. In these articles, optimisation procedures are used to estimate the mechanical parameters μ and α. The optimisation procedure may converge towards a local minimum due to various reasons, such as regions in the parametric space where the simulation fails to converge, a poor choice of algorithm, incorrect algorithm settings (especially step size), inadequate initial guess or because of the topology of the response map, which cannot be visualized during such a procedure. However, the main drawback of the exploration of the parametric space is its computational cost. In this article, a total of 368 879 Finite Element Simulations have been performed representing about 50 days of calculus on a High-Performance Computing platform. The associated carbon footprint has been estimated using the report from the French National Center for Scientific Research (CNRS) (Berthoud et al.,) and was found to be 797 kg eq CO2. As a reminder, the current recommendations for equivalent carbon emissions in France are around 2t eq CO2 per year and per habitants. This highlights the non-negligible environmental cost

associated to the computation costs. In addition to the computational cost, the time required for the identification of soft tissue mechanical properties using an exploration of the functional space is incompatible with the constraints associated with a clinical environment. Recent advances on the use of reduced order models have enabled the estimation of the mechanical properties in real time (Rohan et al., 2023; Song et al., 2022, 2024) Therefore, a further development of this model could be the use of the response map as a basis for model order reduction.

The comparison between the homogenised monolayer and bilayer models revealed that adding a layer reduces the error on the local force displacement curves, thereby increasing the accuracy of the local kinematics of soft tissues during indentation. This, in turn, enhances our understanding of load transmission in soft tissue. However, the benefits of this second layer on the global kinematics of soft tissue appear to be of minor importance. The article demonstrates that the monolayer model may be adequate when examining the global force/displacement relationship. To prevent deep tissue injury, it is necessary to have a thorough understanding of the local mechanical state of the tissue. Therefore, the results of this study encourage the development of characterization procedures that include both muscular and adipose tissue.

The large distance between consecutive values of the shear modulus may be explained by the coarse exploration of the parametric space. This could be the reason why the best shear modulus of muscle tissue is consistently found to be 1.675 kPa for most subjects. The closest possible values of the shear modulus are indeed 0.948 kPa and 2.960 kPa, representing a huge gap between two consecutive values of the μ coefficient.

Also, the comparison of the two models in terms of strains showed that the modelling choice made highly influences the localization of maximal compressive strains (Fig. 10). In terms of strain amplitude, the bilayer model led to reduced maximal compressive strain value and a higher amplitude of shear strain in the ultrasound plane (Fig. 11). As tissue internal strains are related to pressure ulcer risk (Ceelen et al., 2008), both localization and amplitude are important data to consider in a patient specific manner. However, as no experimental data are available on internal strain during indentation, it is difficult to conclude about the choice to make to best represent the *in vivo* strain. Once again, further work should be conducted in the biomechanical community to develop reliable methodologies to estimate *in vivo* strain in soft tissue.

Similarly, it is expected that the homogenised layer of muscle tissue underestimates internal strains. Therefore, increasing the geometric complexity of the model could lead to a more precise estimation of tissue internal strains. Although attempts have been made to develop a model that differentiates between different muscular lodges, the rigid body and out-of-plane motion of these lodges make the models very unstable. Developing patient-specific models requires a better understanding of how muscles attach to bones and how force is transmitted through different muscular lodges by the fascia layers. Increasing the complexity of such a model will deepen the comprehension of the mechanisms that play a role in pressure ulcer development. However, it is important to evaluate the clinical relevance of using such a detailed model to estimate patient-specific constitutive parameters in a clinical setting.

In this contribution, it is assumed that the thickness of the tissues is homogeneous all over the contour. It can be expected that this strong assumption will also affect the strains estimated in the tissues. However, as it is the vertical displacement of points on the interface that is used for the calibration of material properties, it is expected that the inhomogeneity of the thicknesses will not affect the measure of the displacement of the points directly under the ultrasound probe and thus will not affect the experimental force displacement curves.

In a similar way, the contact between the muscle and adipose tissue is modelled by a Tie interaction in this work. Experimental ultrasound clips display (available as supplementary material 2) clearly that a relative motion between the rectus femoris and the adipose tissue exists in the tangential direction until a certain point. This motion is expected to change the estimated values of internal strains in the tissue. However, taking this into account in the model requires to define in a more accurate way the internal geometry of the thigh, and characterize this relative motion allowed by the fascia wrapping the muscle. Further work should focus on such developments.

Moreover, the fact that the same isotropic material constitutive model has been used to described both muscle and fat is questionable. Huge differences can indeed be noticed in the structure of the materials. Muscle is composed of muscle fibers gathered in lodges, making this a highly anisotropic material. On the contrary, adipose tissue seems to be organised into globules with an incompressible behaviour. Further work is required to improve the representation of the different layers of soft tissue. However, it can be expected that the effect of the anisotropy on the estimated 2D strain field could be negligible regarding other strong hypotheses made to construct this model.

A major limitation of this work relies on the fact that indentations are performed using a handheld device and thus that no control is possible on the loading rate applied on the tissue. Regarding the time-dependent aspect of the mechanical response of the soft tissues, it can be expected that the acquisition procedure lacks repeatability. An *a posteriori* verification showed that the loading rate was 7.8 ± 2.5 mm/s, which is quite high for quasi-static assumption. Further work is needed to characterize *in vivo* the time-dependency of the mechanical response.

As the thigh is not an area at risk for pressure ulcers, additional work is required to confirm that the constitutive parameters estimated with the methodology presented in this research are still applicable to areas at risk of developing pressure ulcers. The simple modelling used in the methodology allows to transpose this model to different areas of the body where two layers of different materials are superimposed. However, the simplicity of the model is associated to a lack of accuracy when representing the *in vivo* loading and it is expected that different anatomical differences such as attachment points, composition of the materials can modify the obtained results.

5. Conclusion

This retrospective study presents a methodology for extracting force-displacement curves for the muscle and tissue layers from an ultrasound cyclic indentation clip. To avoid problems associated with the use of an optimisation procedure to find a set of parameters that minimises the distance between the experimental and simulated force-displacement curves, an exploration of the parametric space of material parameters has been carried out using two different finite element models representing the soft tissues as a single and two different layers respectively. The contribution of this paper is that a two-layer model allows a more accurate representation of the force-displacement relationship of the muscle and fat layers. Further work should focus on 1/Improving the characterisation and modelling of the geometry, the interactions between the different parts of the model and the characterisation of the temporal response of the tissue. 2/Further work is also needed to estimate *in vivo* strain from medical imaging for better characterisation and validation of material properties. 3/Finally, the use of the estimated material properties as a tool to identify the population at risk of pressure ulcers will be investigated.

CRediT authorship contribution statement

Alexandre Segain: Writing – original draft, Visualization, Software, Resources, Methodology, Investigation, Formal analysis, Data curation. **Giuseppe Sciume:** Writing – original draft, Supervision, Methodology, Investigation, Funding acquisition, Formal analysis, Conceptualization. **Hélène Pillet:** Writing – original draft, Supervision, Project administration, Methodology, Funding acquisition, Formal analysis, Conceptualization. **Pierre-Yves Rohan:** Writing – original draft, Supervision, Project administration, Methodology, Investigation, Funding acquisition, Formal analysis, Conceptualization.

Declaration of competing interest

The authors declare that they have no known competing financial interests or personal relationships that could have appeared to influence the work reported in this paper.

Data availability

Data will be made available on request.

Acknowledgment

The authors of the manuscript wanted to thank the HPC CASSIOPEE from the Arts et Métiers Institute of Technology.

Appendix A. Supplementary data

Supplementary data to this article can be found online at https://doi.org/10.1016/j.jmbbm.2024.106584.

References

Affagard, J.S., Bensamoun, S.F., Feissel, P., 2014. Development of an inverse approach for the characterization of in vivo mechanical properties of the lower limb muscles. J. Biomech. Eng. 136 (11) https://doi.org/10.1115/1.4028490.

Affagard, J.S., Feissel, P., Bensamoun, S.F., 2015. Identification of hyperelastic properties of passive thigh muscle under compression with an inverse method from a displacement field measurement. J. Biomech. 48 (15), 4081–4086. https://doi.org/10.1016/j.jbiomech.2015.10.007.

Al-Dirini, R.M.A., Reed, M.P., Hu, J., Thewlis, D., 2016. Development and validation of a high anatomical fidelity FE model for the buttock and thigh of a seated individual. Ann. Biomed. Eng. 44 (9), 2805–2816. https://doi.org/10.1007/s10439-016-1560-3.

Avril, S., Bouten, L., Dubuis, L., Drapier, S., Pouget, J.F., 2010. Mixed experimental and numerical approach for characterizing the biomechanical response of the human leg under elastic compression. J. Biomech. Eng. 132 (3) https://doi.org/10.1115/1.4000967.

Barbarino, G.G., Jabareen, M., Mazza, E., 2011. Experimental and numerical study on the mechanical behavior of the superficial layers of the face. Skin Res. Technol. 17 (4), 434–444. https://doi.org/10.1111/j.1600-0846.2011.00515.x.

Berthoud, F., Bzeznik, B., Gibelin, N., Laurens, M., Bonamy, C., Morel, M., & Schwindenhammer, X. (n.d.). Estimation de l'empreinte carbone d'une heure.*coeur de calcul*. https://hal.science/hal-02549565v4.

Böl, M., Kruse, R., Ehret, A.E., Leichsenring, K., Siebert, T., 2012. Compressive properties of passive skeletal muscle-The impact of precise sample geometry on parameter identification in inverse finite element analysis. J. Biomech. 45 (15), 2673–2679. https://doi.org/10.1016/j.jbiomech.2012.08.023.

Call, E., Hetzel, T., McLean, C., Burton, J.N., Oberg, C., 2017. Off loading wheelchair cushion provides best case reduction in tissue deformation as indicated by MRI. J. Tissue Viability 26 (3), 172–179. https://doi.org/10.1016/j.jtv.2017.05.002.

Calvo-Gallego, J.L., Domínguez, J., Gómez Cía, T., Ruiz-Moya, A., Gómez Ciriza, G., Martínez-Reina, J., 2020. Comparison of the viscoelastic properties of human abdominal and breast adipose tissue and its incidence on breast reconstruction surgery. A pilot study. Clin. BioMech. 71, 37–44. https://doi.org/10.1016/j.clinbiomech.2019.10.009.

Ceelen, K.K., Stekelenburg, A., Loerakker, S., Strijkers, G.J., Bader, D.L., Nicolay, K., Baaijens, F.P.T., Oomens, C.W.J., 2008. Compression-induced damage and internal tissue strains are related. J. Biomech. 41 (16), 3399–3404. https://doi.org/10.1016/j.jbiomech.2008.09.016.

Chawla, A., Mukherjee, S., Karthikeyan, B., 2009. Characterization of human passive muscles for impact loads using genetic algorithm and inverse finite element methods. Biomech. Model. Mechanobiol. 8 (1), 67–76. https://doi.org/10.1007/s10237-008-0121-6.

Demarré, L., Van Lancker, A., Van Hecke, A., Verhaeghe, S., Grypdonck, M., Lemey, J., Annemans, L., Beeckman, D., 2015. The cost of prevention and treatment of pressure ulcers: a systematic review. Int. J. Nurs. Stud. 52 (11), 1754–1774. https://doi.org/10.1016/j.ijnurstu.2015.06.006. Elsevier Ltd.

Diab, M., Kumaraswamy, N., Reece, G.P., Hanson, S.E., Fingeret, M.C., Markey, M.K., Ravi-Chandar, K., 2020. Characterization of human female breast and abdominal skin elasticity using a bulge test. J. Mech. Behav. Biomed. Mater. 103 https://doi.org/10.1016/j.jmbbm.2019.103604.

Doridam, J., Macron, A., Vergari, C., Verney, A., Rohan, P.Y., Pillet, H., 2018. Feasibility of sub-dermal soft tissue deformation assessment using B-mode ultrasound for pressure ulcer prevention. J. Tissue Viability 27 (4), 238–243. https://doi.org/10.1016/j.jtv.2018.08.002.

Fougeron, N., Rohan, P.Y., Haering, D., Rose, J.L., Bonnet, X., Pillet, H., 2020. Combining freehand ultrasound-based indentation and inverse finite element modeling for the identification of hyperelastic material properties of thigh soft tissues. J. Biomech. Eng. 142 (9) https://doi.org/10.1115/1.4046444.

Gras, L.L., Mitton, D., Viot, P., Laporte, S., 2012. Hyper-elastic properties of the human sternocleidomastoideus muscle in tension. J. Mech. Behav. Biomed. Mater. 15, 131–140. https://doi.org/10.1016/j.jmbbm.2012.06.013.

Haddad, S.M.H., Dhaliwal, S.S., Rotenberg, B.W., Ladak, H.M., Samani, A., 2020. Estimation of the hyperelastic parameters of fresh human oropharyngeal soft tissues using indentation testing. J. Mech. Behav. Biomed. Mater. 108 https://doi.org/10.1016/j.jmbbm.2020.103798.

Hatt, A., Lloyd, R., Bolsterlee, B., Bilston, L.E., 2023. Strain-dependent shear properties of human adipose tissue in vivo. J. Mech. Behav. Biomed. Mater. 143 https://doi.org/10.1016/j.jmbbm.2023.105924.

Hendriks, F.M., Brokken, D., van Eemeren, J.T.W.M., Oomens, C.W.J., Baaijens, F.P.T., Horsten, J.B.A.M., 2003. A numerical-experimental method to characterize the non-linear mechanical behavior of human skin. Skin Res. Technol. 9 (3), 274–283. https://doi.org/10.1034/j.1600-0846.2003.00019.x.

Isogai, K., Okamoto, S., Asaba, T., Ogusu, S., Shimizu, Y., Watanabe, T., Yamada, Y., 2022. Young's moduli of subcutaneous tissues and muscles under different loads at the gluteal region calculated using ultrasonography. J. Phys. Ther. Sci. 34, 777–783.

Kim, J., Srinivasan, M.A., 2005. Characterization of viscoelastic soft tissue properties from in vivo animal experiments and inverse FE parameter estimation. LNCS 3750, 599–606. www.sensable.com.

Luboz, V., Petrizelli, M., Bucki, M., Diot, B., Vuillerme, N., Payan, Y., 2014a. Biomechanical modeling to prevent ischial pressure ulcers. J. Biomech. 47 (10), 2231–2236. https://doi.org/10.1016/j.jbiomech.2014.05.004.

Luboz, V., Promayon, E., Payan, Y., 2014b. Linear elastic properties of the facial soft tissues using an aspiration device: towards patient specific characterization. Ann. Biomed. Eng. 42 (11), 2369–2378. https://doi.org/10.1007/s10439-014-1098-1.

Mak, A.F.T., George, Liu, H.W., Lee, S.Y., 1994. Department of Veterans Affairs Biomechanical assessment of below-knee residual limb tissue. J. Rehabil. Res. Dev. 31 (Issue 3).

Makhsous, M., Venkatasubramanian, G., Chawla, A., Pathak, Y., Priebe, M., Rymer, W.Z., Lin, F., 2008. Investigation of soft-tissue stiffness alteration in denervated human tissue using an ultrasound indentation system. The Journal of Spinal Cord Medicin 31 (1), 88–96. https://doi.org/10.1080/10790268.2008.11753987.

Moerman, K.M., Van Vijven, M., Solis, L.R., Van Haaften, E.E., Loenen, A.C.Y., Mushahwar, V.K., Oomens, C.W.J., Moerman, K.M., 2017. On the importance of 3D, geometrically accurate, and subject-specific finite element analysis for evaluation of in-vivo soft tissue loads. Comput. Methods Biomech. Biomed. Eng. 20 (5), 483–491. https://doi.org/10.1080/10255842.2016.1250259.

Morrow, D.A., Haut Donahue, T.L., Odegard, G.M., Kaufman, K.R., 2010. Transversely isotropic tensile material properties of skeletal muscle tissue. J. Mech. Behav. Biomed. Mater. 3 (1), 124–129. https://doi.org/10.1016/j.jmbbm.2009.03.004.

Mott, P.H., Dorgan, J.R., Roland, 2008. The bulk modulus and Poisson's ratio of "Incompressible" materials. J. Sound Vib. 312 (4–5), 572–575.

Mukhina, E., Trebbi, A., Rohan, P.Y., Connesson, N., Payan, Y., 2022. In vivo quantification of 3D displacement in sacral soft tissues under compression: relevance of 2D US-based measurements for pressure ulcer risk assessment. J. Tissue Viability 31 (4), 593–600. https://doi.org/10.1016/j.jtv.2022.09.007.

Oddes, Z., Solav, D., 2023. Identifiability of soft tissue constitutive parameters from in-vivo macro-indentation. J. Mech. Behav. Biomed. Mater. 140 https://doi.org/10.1016/j.jmbbm.2023.105708.

Ogden, R.W., 1973. Large deformation isotropic elasticity—on the correlation of theory and experiment for incompressible rubberlike solids. Rubber Chem. Technol. 46 (2), 398–416.

Omidi, E., Fuetterer, L., Reza Mousavi, S., Armstrong, R.C., Flynn, L.E., Samani, A., 2014. Characterization and assessment of hyperelastic and elastic properties of decellularized human adipose tissues. J. Biomech. 47 (15), 3657–3663. https://doi.org/10.1016/j.jbiomech.2014.09.035.

Oomens, C.W.J., Zenhorst, W., Broek, M., Hemmes, B., Poeze, M., Brink, P.R.G., Bader, D.L., 2013. A numerical study to analyse the risk for pressure ulcer development on a spine board. Clin. BioMech. 28 (7), 736–742. https://doi.org/10.1016/j.clinbiomech.2013.07.005.

Rohan, P.-Y., Fougeron, N., Keenan, B., Pillet, H., Laporte, S., Osipov, N., Ryckelynck, D., 2023. Real-time numerical prediction of strain localization using dictionary-based ROM-nets for sitting-acquired deep tissue injury prevention. In: Reduced Order Models for the Biomechanics of Living Organs. Elsevier, pp. 385–402. https://doi.org/10.1016/B978-0-32-389967-3.00027-5.

Samani, A., Bishop, J., Luginbuhl, C., Plewes, D.B., 2003. Measuring the elastic modulus of ex vivo small tissue samples. Phys. Med. Biol. 48, 2183–2198.

Silber, G., Then, C., 2013. Preventive biomechanics: optimizing support systems for the human body in the lying and sitting position. In: Preventive Biomechanics: Optimizing Support Systems for the Human Body in the Lying and Sitting Position. Springer Berlin Heidelberg. https://doi.org/10.1007/978-3-642-29003-9.

Sommer, G., Eder, M., Kovacs, L., Pathak, H., Bonitz, L., Mueller, C., Regitnig, P., Holzapfel, G.A., 2013. Multiaxial mechanical properties and constitutive modeling of human adipose tissue: a basis for preoperative simulations in plastic and reconstructive surgery. Acta Biomater. 9 (11), 9036–9048. https://doi.org/10.1016/j.actbio.2013.06.011.

Sonenblum, S.E., Sprigle, S.H., Cathcart, J.M.K., Winder, R.J., 2015. 3D anatomy and deformation of the seated buttocks. J. Tissue Viability 24 (2), 51–61. https://doi.org/10.1016/j.jtv.2015.03.003.

Song, J., Xie, H., Zhong, Y., Gu, C., Choi, K.S., 2023. Maximum likelihood-based extended Kalman filter for soft tissue modelling. J. Mech. Behav. Biomed. Mater. 137 https://doi.org/10.1016/j.jmbbm.2022.105553.

Song, J., Xie, H., Zhong, Y., Gu, C., Choi, K.S., 2024. Dynamic Mode Decomposition for soft tissue deformation modelling. Appl. Math. Model. 127, 60–70. https://doi.org/10.1016/j.apm.2023.11.019.

Song, J., Xie, H., Zhong, Y., Li, J., Gu, C., Choi, K.S., 2022. Reduced-order extended kalman filter for deformable tissue simulation. J. Mech. Phys. Solid. 158 https://doi.org/10.1016/j.jmps.2021.104696.

Then, C., Vogl, T.J., Silber, G., 2012. Method for characterizing viscoelasticity of human gluteal tissue. J. Biomech. 45 (7), 1252–1258. https://doi.org/10.1016/j.jbiomech.2012.01.037.

Tran, H.V., Charleux, F., Rachik, M., Ehrlacher, A., Ho Ba Tho, M.C., 2007. In vivo characterization of the mechanical properties of human skin derived from MRI and indentation techniques. Comput. Methods Biomech. Biomed. Eng. 10 (6), 401–407. https://doi.org/10.1080/10255840701550287.

Vaidya, A.J., Wheatley, B.B., 2020. An experimental and computational investigation of the effects of volumetric boundary conditions on the compressive mechanics of passive skeletal muscle. J. Mech. Behav. Biomed. Mater. 102 https://doi.org/10.1016/j.jmbbm.2019.103526.

Vergari, C., Mansfield, J., Meakin, J.R., Winlove, P.C., 2016. Lamellar and fibre bundle mechanics of the annulus fibrosus in bovine intervertebral disc. Acta Biomater. 37, 14–20. https://doi.org/10.1016/j.actbio.2016.04.002.

Zhu, X., Gao, B., Zhong, Y., Gu, C., Choi, K.S., 2021. Extended Kalman filter for online soft tissue characterization based on Hunt-Crossley contact model. J. Mech. Behav. Biomed. Mater. 123 https://doi.org/10.1016/j.jmbbm.2021.104667.

Zhu, X., Li, J., Zhong, Y., Choi, K.S., Shirinzadeh, B., Smith, J., Gu, C., 2023. Iterative Kalman filter for biological tissue identification. Int. J. Robust Nonlinear Control. https://doi.org/10.1002/rnc.6742.